https://doi.org/10.22226/2410-3535-2022-4-379-384

Effect of rare-earths (La, Nd, Pr) on zirconate ceramics for thermal barrier coatings

S. A. Oglezneva, S. E. Porozova, M. N. Kachenyuk, A. A. Smetkin, V. B. Kul'met'eva†

†kulmetevavb@pstu.ru

Perm National Research Polytechnic University, Perm, 614990, Russia

Zirconium oxide-based powders with different concentrations of REE concentrate (La, Nd, Pr) in an amount from 25 to 35 mol.% were synthesized by the reverse chemical precipitation method. The formation of REE zirconates during consolidation has been studied by Raman spectroscopy, XRD and scanning electron microscopy. It has been established that the formation of REE zirconates with the pyrochlore structure occurs after annealing of synthesised powders at a temperature of 1000°C. It has been demonstrated that densifying processes during sintering at 1400–1600°C occur most slowly in a ceramic material with 35 mol.% REE oxides, which has a stable phase composition at all sintering temperatures, consisting mainly of REE zirconates with the pyrochlore structure. The resulting ceramic material based on REE zirconates has phase stability at 1300°C.

Keywords: rare-earth metal oxides, pyrochlore, pyrochlore-fluorite transformation, thermal barrier coatings.

1. Introduction

The zirconates of rare-earth elements (REE) with the general formula $Ln_2Zr_2O_7$ (where Ln is a trivalent rare-earth element or lanthanide), which have high melting temperatures, thermal stability, ionic conductivity, radiation resistance, and low thermal conductivity, are used as new solid electrolytes with high oxygen-ionic conductivity for high-temperature solid oxide fuel cells [1,2], oxidation catalysts and sensors [3–5], for immobilisation of radioactive waste of nuclear power installations [6,7]. It is worth noting their potential as materials for thermal barrier coatings (TBC) working at temperatures above 1200°C [8–13].

Two crystal structures characterise these materials: fluorite ($Fm\bar{3}m$, $Z=4$) and pyrochlore ($Fd\bar{3}m$, $Z=8$). In the series of REE zirconates, zirconates of the first half of the La-Gd series have the pyrochlore structure, and zirconates of the second half of the Tb-Lu series have the fluorite structure. The structure of REE zirconates strongly depends on the ratio of Ln^{3+} and Zr^{4+} radii. If this ratio is within the interval $1.46 \le r(Ln^{3+})/r(Zr^{4+}) \le 1.78$, the ordered pyrochlore structure is stable. Some of these materials may undergo an order-disorder phase transformation from pyrochlore to fluorite at temperatures above 1500°C. This thermal transition depends on the nature of the rare-earth ion [8,14,15].

Some physical properties of REE zirconates depend linearly on their chemical composition, so the lattice parameters of $Ln_2Zr_2O_7$ with the pyrochlore structure increase with the Ln ionic radius, and the melting temperature, on the contrary, decreases [16]. The thermal conductivity value also depends on the cationic radius that is important for their use as a material for TBC [8,9]. The study carried out in [17] demonstrates that thermal expansion of $Ln_2Zr_2O_7$ (Ln = La, Nd, Sm, Gd, Dy, Y) becomes smaller with the increasing Ln ionic radius. Therefore, to change the properties of REE zirconates, joint doping with various cations of REE is widely used, which creates defect clusters that increase the scattering of phonons and thus reduce the thermal conductivity of pyrochlore phases [10]. For example, in [18], joint doping of $La_2Zr_2O_7$ with one or several oxides (Gd_2O_3, Yb_2O_3) resulted in a lower thermal conductivity, and in [19], it resulted in the partial substitution of cation La^{3+} for cations Dy and Nd, and cations Zr^{4+} for Ce, and a reduction in thermal conductivity was also achieved. The temperature coefficient of linear expansion (TCE) of $Nd_2Zr_2O_7$ was increased from $10.68 \cdot 10^{-6}$ K^{-1} to $11.29 \cdot 10^{-6}$ K^{-1} due to doping with 10 mol.% Sc_2O_3 [20]. $Gd_2Zr_2O_7$ doped with Yb_2O_3 also showed lower thermal conductivity and higher TCE, increasing the content of Yb_2O_3 [21].

Currently, one of the research trends in ceramic materials for the next-generation TBCs is the development of high-entropy oxide ceramics [22–24] in the form of solid solutions containing three or more stoichiometrical components in equal or almost equal molar ratios. The studies of a high-entropy solid solution of the composition developed in [25] $(La_{0.2}Ce_{0.2}Nd_{0.2}Sm_{0.2}Eu_{0.2})_2Zr_2O_7$ showed that its thermal conductivity at room temperature was only 0.76 W/m·K. Thermal conductivity below 1 W/m·K in the temperature range of 300–1200°C is demonstrated by high-entropy ceramics with the pyrochlore structure obtained by solid-phase synthesis by mixing five of the six REE oxides (La_2O_3, Nd_2O_3, Sm_2O_3, Eu_2O_3, Gd_2O_3, and Y_2O_3) with equimolar ratio and ZrO_2 [26]. Zhou et al used high-entropy REE zirconate $(La_{0.2}Nd_{0.2}Sm_{0.2}Eu_{0.2}Gd_{0.2})_2Zr_2O_7$ as the upper layer in a two-layer coating with zirconium oxide stabilised by yttrium oxide (YSZ) [27]. Thermocycling tests at 1100°C in air showed that the resulting coating had better thermal stability compared to the $La_2Zr_2O_7$/YSZ coating. The authors of [28] show that ionic radii, valence, and dimensional disorder can be the main driving forces for the formation of single-phase high-entropy

oxides, and by changing the elemental composition, we can manage the synthesis of high-entropy ceramic materials with the structure of pyrochlore or fluorite.

In [29], a ceramic layer was studied that was based on ZrO_2 doped with the mixture of REE oxides represented by REE concentrate based on CeO_2. The authors believe that the simultaneous use of REE oxides with cations of various sizes and valence results in a solid solution with a strongly imperfect structure, which can be a prerequisite for the production of ceramics with a low thermal conductivity required for the ceramic layer of the fuel assembly.

This study aims to investigate the formation of ceramic heat-shielding materials thermally stable at 1300°C, which are based on zirconates and use a concentrate of rare-earth elements.

2. Materials and experimental methods

Powders for the synthesis of zirconates were obtained by inverse coprecipitation of freshly prepared 0.5 M aqueous solution of salt $ZrOCl_2 \cdot 8H_2O$ of pure qualification. As the source of rare-earth elements, we used REE concentrate in the form of carbonates manufactured by OJSC Solikamsk Magnesium Plant (Russia), with the following oxide content (mass%): La_2O_3 — 61.2; Nd_2O_3 — 25.5; Pr_6O_{11} — 10.3; CeO_2 — 0.0065; Nb_2O_5 — 0.09; CaO — 0.67; SrO — 0.05; Fe_2O_3 — 0.02; TiO_2 — 0.10. The content of REE oxides calculated on the ZrO_2-La_2O_3 phase diagram ranged in the amount of 25, 30, and 35 mol.% [16].

The REE concentrate was dissolved in the concentrated HNO_3 with heating. Coprecipitation was carried out while maintaining pH 9–10 of the reaction medium. One per cent aqueous solution of ammonia was used as a precipitator. The resulting gelled precipitate was washed from Cl^- and NH^{4+} ions with distilled water. The precipitate dried in air at $T = 50$°C was ground in a planetary mill at a rotation rate of 160 rpm for 1 hour in the ethanol medium. The heat treatment of pre-dried and ground powders was performed at $T = 600–1200$°C/60 min in the air atmosphere. Synthesis of phases during heating proceeds in accordance with the typical reaction: $Ln_2O_3 + 2ZrO_2 \rightarrow Ln_2Zr_2O_7$.

The samples were pressed by the method of cold uniaxial pressing at a pressure of 150 MPa. Before pressing, the powders were subjected to annealing at 600°C/1 h. Sintering in the temperature range of 1400–1600°C with exposure for 2 h and isothermal exposure at 1300°C for 50 h was carried out in the air in high-temperature electrical resistance furnace HT 64/17 (Nabertherm GmbH).

The phase composition of the samples was studied by Raman spectroscopy (SENTERRA, Bruker) at $\lambda = 532$ nm and by using XRD-ray (XRD-6000, Shimadzu) with CuK_α radiation in the range of 10–90 in steps of 0.02. Interpretation of diffraction patterns was carried out on the basis of an ICDD (International Centre for Diffraction Data) PDF-2 licensed data-base. The apparent density and open porosity were determined by Archimedes method using deionized water as the immersion medium. The microstructure analysis of the sintered samples was carried out by a scanning electron microscope VEGA3 (TESCAN) on the sections after high-temperature etching.

3. Results and discussion

We studied the effect of annealing in the temperature range of 600–1200°C on the phase composition of the powder depending on the content of REE oxides (Fig. 1). It has been established that after annealing at 600°C, all powders are in an amorphous state. Due to its structural similarity,

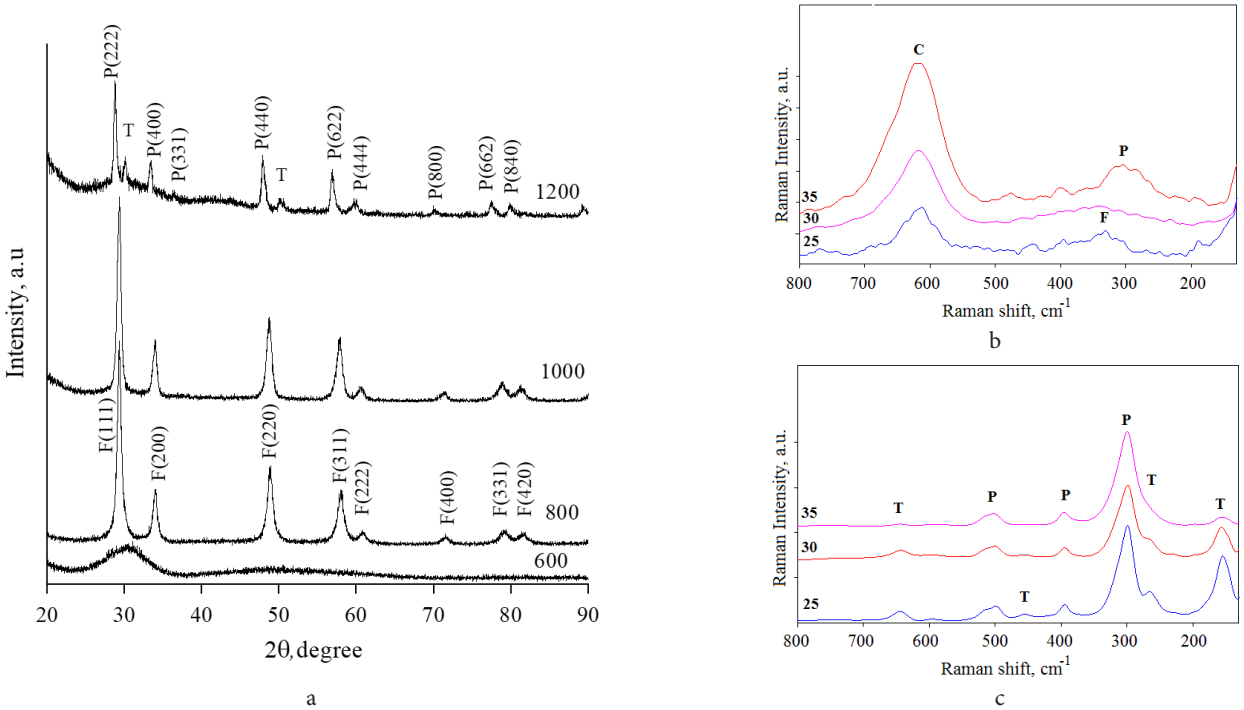

Fig. 1. (Color online) XRD patterns of powders with 25 mol.% REE oxides after annealing at different temperatures (a) and Raman spectra of synthesized powders with different content of REE oxides after annealing for 1 h at a temperature: 800°C (b), 1200°C (c). C — cubic ZrO_2; T — tetragonal ZrO_2; P — pyrochlore; F — fluorite.

it is difficult to distinguish fluorite from pyrochlore phase by XRD analysis. To differentiate pyrochlore from fluorite, Bragg reflections (111), (311), (331), (511) arising from the superstructure of pyrochlore phase are used. However, the intensity of these peaks is insignificant compared to the main phase and therefore is not visible after annealing at 800°C, since it contains the dominant fluorite phase. Raman spectroscopy was used to distinguish between the fluorite and pyrochlore phases, as it allows one to effectively investigate the local ordering in the system. In the Raman spectrum of powders with a content of 25 – 30 mol.% of REE oxides a wide peak of low intensity can be distinguished at 340 cm^{-1}, which the authors [30] attribute to the only active Raman mode of zirconate with an unordered fluorite structure (Fig. 1b). In the spectrum of powder with 35 mol.% REE mode of pyrochlore is fixed (300 cm^{-1}). Raman spectra of the compounds of $A_2B_2O_7$ type with the pyrochlore structure are characterised by the presence of six active modes ($A_{1g}+E_g+4F_{2g}$), the main of which are 300 cm^{-1} (E_g), 395 cm^{-1} (F_{2g}), 492 cm^{-1} (A_{1g}), 516 cm^{-1} (F_{2g}) [31–34]. The greatest intensity is characteristic for line ≈300 cm^{-1}, which according to [35,36] consists of two lines of different intensities with very close wavenumbers, which is confirmed by the calculations *ab initio* in [37,38], where the frequencies and types of phonon modes were determined for $La_2Zr_2O_7$ and $Nd_2Zr_2O_7$. After annealing at 1000°C, the appearance of lines corresponding to zirconates with the pyrochlore structure of all compositions is noted in the spectrum. Further increase in the annealing temperature to 1200°C leads to narrowing the mainline of zirconates (300 cm^{-1}), suggesting the formation of a more advanced crystal structure. The strongest lines are recorded in the spectrum corresponding to the tetragonal zirconium dioxide (150, 265, 644 cm^{-1}) [39,40], the intensity of which decreases with the increasing content of REE oxides (Fig. 1c).

Thus, the formation of REE zirconates with the pyrochlore structure occurs above 1000°C, which agrees well with the results obtained in [30,33,34].

After moulding, the apparent density of the compacts was in the range 2.91–3.15 g/cm^3. After sintering at 1400°C, the density of all samples is quite low: the open porosity is 35 – 40% (Table 1), although the bulk shrinkage of samples with 25 mol.% REE oxides is rather high, up to 31%. The increase in the sintering temperature to 1500°C led to a significant decrease in the open porosity: more than four-fold for ceramics with 25 mol.% REE oxides and two-fold for ceramics with 30 mol.% REE oxides. With this, the apparent density of these ceramics has the maximum value. Ceramics with 35 mol.% REE reaches the highest density only after sintering at 1600°C, and the open porosity is 12 – 15%. At the same time, ceramics with a lower content of REE oxides showed a decrease in the apparent density and volume shrinkage.

Table 1. Dependence of apparent density and open porosity on sintering temperature of ceramics based on REE zirconates.

REE oxides content, mol.%	Temperature, °C	Apparent density, g/cm^3	Open porosity, %
25	1400	3.95 ± 0.01	34.5 ± 0.2
	1500	5.33 ± 0.03	8.1 ± 0.4
	1600	4.04 ± 0.03	15.0 ± 0.4
30	1400	3.87 ± 0.02	34.7 ± 2.2
	1500	5.00 ± 0.01	17.4 ± 0.4
	1600	4.63 ± 0.06	12.1 ± 0.5
35	1400	3.49 ± 0.01	40.7 ± 0.3
	1500	3.68 ± 0.01	37.0 ± 0.2
	1600	4.65 ± 0.04	14.1 ± 0.4

According to the Raman spectroscopy, after sintering at 1400°C, the phase composition of all samples, except for REE zirconates with the pyrochlore structure, contains tetragonal ZrO_2, the amount of which decreases with an increase in the content of REE oxides (Fig. 2a). The decomposition of the wide line with its maximum at 300 cm^{-1} by the Levenberg-Marquardt algorithm showed that it consisted of lines corresponding to the maximum in intensity line of lanthanum neodymium zirconates with the pyrochlore structure (300 cm^{-1}) and the lines of tetragonal zirconium oxide (269 and 312 cm^{-1}) (Fig. 2a, insert).

With an increase in the sintering temperature to 1500°C, lines 178 and 190 cm^{-1} corresponding to monoclinic ZrO_2 appear in the Raman spectra of ceramics with 25 and 30 mol.% REE oxides. The Raman spectrum of ceramics with 35 mol.% REE oxides remains unchanged, i.e., the phase composition almost completely consists of a zirconate with the pyrochlore structure with a minor amount of tetragonal zirconium

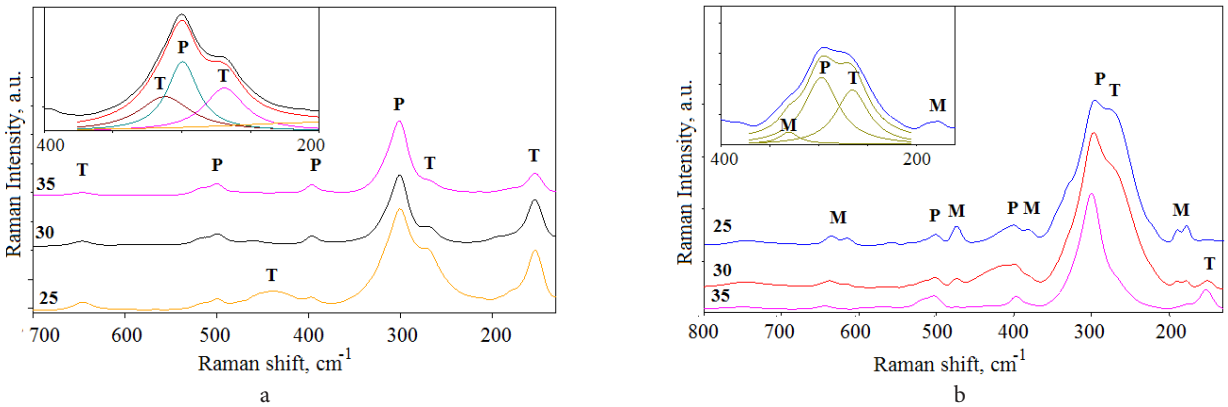

a b

Fig. 2. (Color online) Raman spectra of ceramics with different content of PEE oxides after sintering at 1400°C (a) and 1600°C (b): M — monoclinic ZrO_2, T — tetragonal ZrO_2, P — pyrochlore. Insert: decomposition of line 300 cm^{-1} of the Raman spectrum of the sample with 25 mol.% REE.

dioxide. After sintering at 1600°C, the amount of monoclinic ZrO_2 increases in ceramics with 25 and 30 mol.% REE oxides, as the intensity of lines 178 and 190 cm^{-1} is growing, and other lines corresponding to it also appear in the spectrum (Fig. 2 b). One should note a change in the shape of the line at 300 cm^{-1} caused by the growing intensity of line 269 cm^{-1} of the tetragonal ZrO_2. A decrease in the apparent density of ceramics with 25 and 30 mol.% REE oxides is associated with an increase in the amount of monoclinic ZrO_2. The phase transition from tetragonal to monoclinic ZrO_2 is accompanied by an increase in volume by 4 – 5%, while the theoretical density decreases from 6.1 to 5.8 g/cm^3 resulting in the formation of microcracks [41, 42]. The phase composition of ceramics with 35 mol.% REE oxides remains unchanged.

After sintering at 1500 and 1600°C, the microstructure of all samples consists of polyhedral grains, the size of which depends on the content of REE oxides and the sintering temperature (Fig. 3). The microstructure of ceramics with 25 and 30 mol.% REE oxides contains both large grains up to 2 μm and disperse discharges, the size of which does not exceed 0.3 μm, which is apparently due to the formation of zirconium dioxide. Ceramics with 35 mol.% REE oxides consist of agglomerates of grains of the average size 0.4 μm, and there are almost no disperse discharges. The increase in the sintering temperature leads to a significant increase in ceramics grain, regardless of the content of REE oxides, but ceramics with 35 mol.% REE oxides have the smallest grain size.

Then the effect of isothermal exposure duration at 1300°C in air on the phase composition of the samples sintered at 1600°C was studied. Figure 4 a shows the Raman spectra of ceramics after exposure at 1300°C for 10 hours. These spectra do not significantly differ from the Raman spectra of the initial samples (Fig. 2 b). However, decomposition of the line with the maximum intensity at 300 cm^{-1} has demonstrated that after isothermal exposure for 10 h, ceramics with 25 mol.% REE oxides had a 10% decrease in the integrated intensity of the phase with the pyrochlore structure due to the increase in the total intensity of the monoclinic and tetragonal zirconium oxide.

Ceramics with 30 mol.% REE oxides had a decrease in the integrated intensity of the tetragonal phase, that caused an increase in the intensity of the monoclinic phase, and slight growth in the intensity of the phase with the pyrochlore structure was noted. Another line (320 cm^{-1}) corresponding to the tetragonal zirconium oxide was recorded for ceramics with 35 mol.% REE oxides. Isothermal exposure for 10 h resulted in a significant (by 18.2%) decrease in the integrated intensity of the line of REE zirconate with the pyrochlore structure and accordingly in the increase in the intensity of the line of the tetragonal zirconium oxide.

The increase in the duration of isothermal exposure resulted in a significant change in the phase composition of ceramics with 25 and 30 mol.% of REE oxides, which is reflected in the growing intensity of the lines of monoclinic zirconium oxide (179 and 190 cm^{-1}) and the occurrence of its other lines in the range of 500 – 600 cm^{-1}. Phase composition stabilisation is noted for ceramics with 35 mol.% REE oxides, which is suggested by the quantitative ratio of the integrated intensity of the lines making up the peak at 300 cm^{-1} of the Raman spectrum, which became virtually equal to the initial value prior to isothermal exposure.

The density of ceramics samples with 25 mol.% REE oxides decreased after isothermal exposure for 50 h accompanied by an increase in the open porosity. The density of ceramics

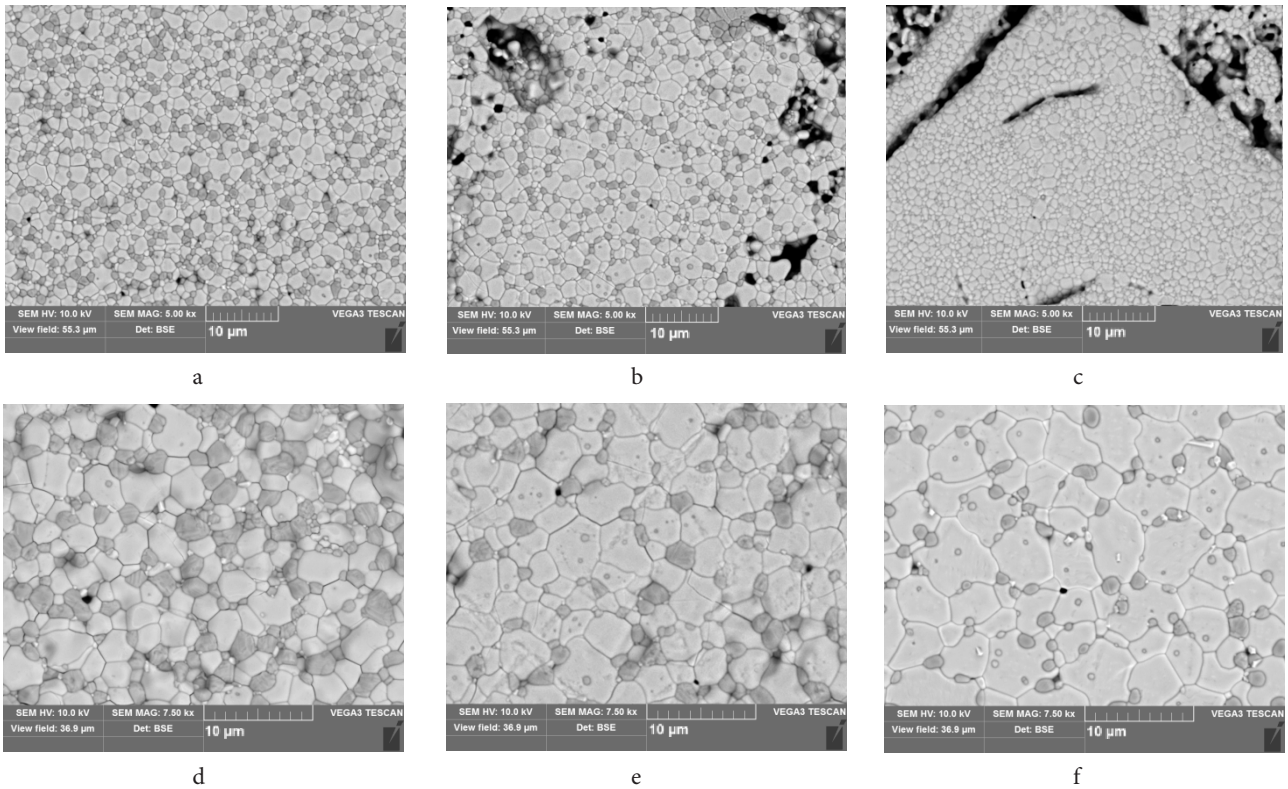

Fig. 3. SEM images of the microstructure of ceramics based on REE zirconates after sintering at temperatures: 1500°C (a – c); 1600°C (d – f); 25 mol.% (a, d), 30 mol.% (b, e), 35 mol.% (c, f) REE oxides. Light gray — rare-earth zirconate, gray — ZrO_2.

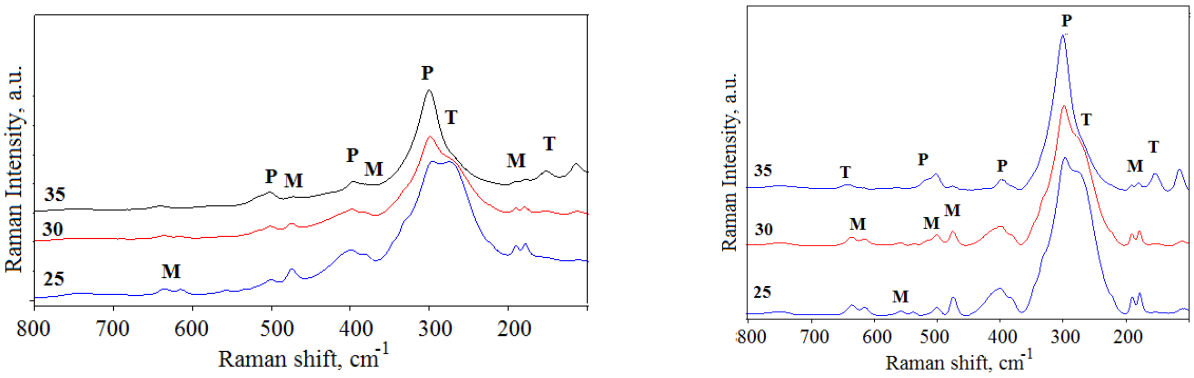

Fig. 4. (Color online) Raman spectra of ceramics with different content of REE oxides after isothermal exposure at 1300°C for: 10 h (a); 50 h (b). M — monoclinic ZrO_2, T — tetragonal ZrO_2, P — pyrochlore.

Table 2. The density and porosity of ceramics samples with different contents of REE oxides after sintering and isothermal exposure at 1300°C for 50 h.

REE oxides content, mol.%	After sintering		After isothermal exposure for 50 h	
	Density, g/cm³	Open porosity, %	Density, g/cm³	Open porosity, %
25	4.04 ± 0.03	15.0 ± 0.4	3.92 ± 0.30	18.6 ± 4.5
30	4.63 ± 0.06	12.1 ± 0.5	4.65 ± 0.23	15.3 ± 1.6
35	4.65 ± 0.04	14.1 ± 0.4	4.62 ± 0.03	18.5 ± 0.9

samples with 30 and 35 mol.% REE oxides practically did not change, but the open porosity value slightly increased (Table 2). This is due to the tetragonal zirconium oxide in the composition of ceramics, which undergoes a polymorphic transformation into monoclinic modification, the amount of which grows with the increasing exposure duration.

4. Conclusion

The powders based on ZrO_2 with different contents of REE concentrate were synthesised by inverse chemical deposition. The concentrate in the form of carbonates was a complex source of La, Nd, and Pr. It has been established that the formation of REE zirconates with the pyrochlore structure occurs after annealing at 1000°C. At higher annealing temperatures, the presence of tetragonal ZrO_2 was noted in the samples with a smaller content of the concentrate in the phase composition. It has been demonstrated that densifying processes during sintering of the single-phase ceramics consisting of zirconates with the pyrochlore structure proceed more slowly, and it has a stable phase composition at all sintering temperatures. After sintering, the microstructure of the ceramics consists of polyhedral grains, the size of which increases with the increasing sintering temperature. The resulting ceramic material based on the REE zirconates, being practically monophase, consisting of REE zirconates with the pyrochlore structure, has a phase and structural stability at isothermal exposure to 1300°C compared to ceramics with a smaller content of REE oxides. The presence of the second phase in the form of the tetragonal ZrO_2 at the long-term isothermal exposure results in its destabilisation and the formation of monoclinic ZrO_2. The use of REE oxides concentrate is promising for obtaining the ceramic layer of heat-shielding coatings with thermal stability at temperatures above 1200°C.

Acknowledgements. The study was carried out within the framework of the public assignment of the Ministry of Education and Science of Russia No. FSNM-2020-0026 for basic scientific research and with financial support from the Russian Foundation for Basic Research, grant No. 19-48-590007.

References

1. A. V. Shlyakhtina, L. G. Shcherbakova. Russ. J. Electrochem. 48 (1), 25 (2012). Crossref
2. A. P. Anantharaman, H. P. Dasari. Ceram. Int. 47 (4), 4367 (2021). Crossref
3. Y. Tong, L. Lu, X. Yang, X. Wang. Solid State Sci. 10 (10), 1379 (2008). Crossref
4. Q. Wang, X. Cheng, J. Li, H. Jin. J. Photochem. Photobiol. A. 321, 48 (2016). Crossref
5. I. Petrila, K. Popa, F. Tudorache. Sens. Actuators. A. 247, 156 (2016). Crossref
6. R. Devanathan, W. J. Weber, J. D. Gale. Energy Environ. Sci. 3 (10), 1551 (2010). Crossref
7. Y. Lu, Q. Peng, C. Liu. Crystals. 11 (6), 667 (2021). Crossref
8. J. Zhang, X. Guo, Y.-G. Jung, L. Li, J. Knapp. Surf. Coat. Technol. 323 (10), 18 (2017). Crossref
9. W. Pan, S. R. Phillpot, C. Wan, A. Chernatynskiy, Z. Qu. MRS Bull. 37, 917 (2012). Crossref
10. X. Cao. J. Mater. Sci. Technol. 23 (1), 15 (2007).
11. I. V. Mazilin, L. Kh. Baldaev, D. V. Drobot, E. Yu. Marchukov, A. M. Akhmetgareeva. Inorg. Mater. 52 (9), 939 (2016). Crossref
12. R. Vaßen, M. O. Jarligo, T. Steinke, D. E. Mack, D. Stöver. Surf. Coat. Technol. 205 (4), 938 (2010). Crossref
13. S. Wu, Y. Zhao, W. Li, W. Liu, Y. Wu, F. Liu. Coatings. 11 (1), 79 (2021). Crossref
14. A. V. Shlyakhtina. Crystallogr. Rep. 58 (4), 548 (2013). Crossref

15. B. P. Mandal, A. Banerji, V. Sathe, S. K. Deb, A. K. Tyagi. J. Solid State Chem. 180 (10), 2643 (2007). Crossref
16. E. R. Andrievskaya. J. Eur. Ceram. Soc. 28 (12), 2363 (2008). Crossref
17. K. Shimamura, T. Arima, K. Idemitsu, Y. Inagaki. Int. J. Thermophys. 28, 1074 (2007). Crossref
18. N. P. Bansal, D. Zhu. Mater. Sci. Eng. A. 459 (1-2), 192 (2007). Crossref
19. H. Zhou, D. Yi. J. Rare Earths. 26 (6), 770 (2008). Crossref
20. L. Guo, Y. Zhang, C. Wang, X. Zhao, F. Ye. Mater. Des. 82, 114 (2015). Crossref
21. L. Guo, H. Guo, H. Peng, S. Gong. J. Eur. Ceram. Soc. 34 (5), 1255 (2014). Crossref
22. Ch. M. Rost, E. Sachet, T. Borman, A. Moballegh, El. C. Dickey, D. Hou, J. L. Jones, S. Curtarolo, M. Jon-Paul. Nat. Commun. 6, 8485 (2015). Crossref
23. S. Jiang, T. Hu, J. Gild, N. Zhou, J. Nie, M. Qin, T. Harrington, K. Vecchio, J. Luo. Scripta Mater. 142, 116 (2018). Crossref
24. R.-J. Zhang, M. J. Reece. J. Mater. Chem. A. 7, 22148 (2019). Crossref
25. Z. Zhao, H. Xiang, F.-Z. Dai, Z. Peng, Y. Zhou. J. Mater. Sci. Technol. 35 (11), 2647 (2019). Crossref
26. F. Li, L. Zhou, J.-X. Liu, Y. Liang, G.-J. Zhang. J. Adv. Ceram. 8 (4), 576 (2019). Crossref
27. L. Zhou, F. Li, J.-X. Liu, Q. Hu, W. Bao, Y. Wu, X. Cao, F. Xu, G.-J. Zhang. J. Eur. Ceram. Soc. 40 (15), 5731 (2020). Crossref
28. Z. Teng, Y. Tan, S. Zeng, Y. Meng, C. Chen, X. Han, H. Zhang. J. Eur. Ceram. Soc. 41 (6), 3614 (2021). Crossref
29. O. V. Dudnik, S. M. Lakiza, I. M. Grechanyuk, V. P. Red'ko, M. S. Glabay, V. B. Shmibelsky, I. O. Marek, A. K. Ruban, M. I. Grechanyuk. Powder Metall. Met. Ceram. 59 (9-10), 556 (2021). Crossref
30. B. Paul, K. Singh, T. Jaroń, A. Roy, A. Chowdhury. J. Alloys Compd. 686, 130 (2016). Crossref
31. S. Wang, W. Li, S. Wang, Z. Chen. J. Eur. Ceram. Soc. 35 (1), 105 (2015). Crossref
32. Ch. Kaliyaperumal, A. Sankarakumar, J. Palanisamy, T. Paramasivam. Mater. Lett. 228, 493 (2018). Crossref
33. L. Kong, I. Karatchevtseva, D. J. Gregg, M. G. Blackford, R. Holmes, G. Triani. J. Eur. Ceram. Soc. 33 (15-16), 3273 (2013). Crossref
34. L. Kong, I. Karatchevtseva, D. J. Gregg, M. G. Blackford, R. Holmes, G. Triani. J. Am. Ceram. Soc. 96 (3), 935 (2013). Crossref
35. A. Panghal, P. K. Kulriya, Y. Kumar, F. Singh, N. L. Singh. Appl. Phys. A. 125, 428 (2019). Crossref
36. G. Sattonnay, N. Sellami, L. Thomé, C. Legros, C. Grygiel, I. Monnet, J. Jagielski, I. Jozwik-Biala, P. Simon. Acta Mater. 61 (17), 6492 (2013). Crossref
37. V. A. Chernyshev. Opt. Spectrosc. 127 (5), 825 (2019). Crossref
38. V. A. Chernyshev. Magn. Reson. Solids Electronic Journal. 21 (4), 19406 (2019). Crossref
39. X. Tang, X. Zheng. J. Mater. Sci. Technol. 20 (5), 485 (2004).
40. Y. Hemberger, N. Wichtner, Ch. Berthold, K. G. Nickel. Int. J. Appl. Ceram. Technol. 13 (1), 116 (2016). Crossref
41. B. Basu. Int. Mater. Rev. 50 (4), 239 (2005). Crossref
42. R. H. J. Hannink, P. M. Kelly, B. C. Muddle. J. Am. Ceram. Soc. 83 (3), 461 (2000). Crossref